Automatic Segmentation of Microcalcification Clusters

Nashid Alam[1(✉)], Arnau Oliver[2], Erika R. E. Denton[3], and Reyer Zwiggelaar[1]

[1] Department of Computer Science,
Aberystwyth University, Aberystwyth, Wales, UK
{naa28,rrz}@aber.ac.uk
[2] Institute of Computer Vision and Robotics, University of Girona, Girona, Spain
aoliver@eia.udg.edu
[3] Norfolk and Norwich University Hospital, Norwich, UK
erika.denton@nnuh.nhs.uk

Abstract. Early detection of microcalcification (MC) clusters plays a crucial role in enhancing breast cancer diagnosis. Two automated MC cluster segmentation techniques are proposed based on morphological operations that incorporate image decomposition and interpolation methods. For both approaches, initially the contrast between the background tissue and MC cluster was increased and subsequently morphological operations were used. Evaluation was based on the Dice similarity scores and the results of MC cluster classification. A total number of 248 (131 benign and 117 malignant) and 24 (12 benign and 12 malignant) biopsy-proven digitized mammograms were considered from the DDSM and MIAS databases, which showed a classification accuracy of $94.48 \pm 1.11\%$ and $100.00 \pm 0.00\%$ respectively.

Keywords: Breast cancer · Microcalcification cluster · Segmentation
Digitized mammogram · Morphological analysis

1 Introduction

Breast cancer is the most common type of cancer in women, and it is considered as one of the major cause of female cancer-related deaths worldwide [1]. The incidence of breast cancer is increasing in developed as well as developing countries [2]. Microcalcification (MC) clusters are small granular deposits of calcium that appear in a mammogram as bright dots, see Fig. 1 for typical examples. The detection of MC clusters can be difficult, especially in dense tissues [3]. Therefore, the MC cluster segmentation is considered as one of the most significant aspect when it comes to computer aided diagnosis (CADx) systems, as the precise segmentation of MC cluster impacts the feature extraction and classification accuracy.

In literature, MC clusters have been segmented using several techniques, such as morphological filters [4–6], machine learning [7,8], the wavelet transform

M. Nixon et al. (Eds.): MIUA 2018, CCIS 894, pp. 251–261, 2018.
https://doi.org/10.1007/978-3-319-95921-4_24

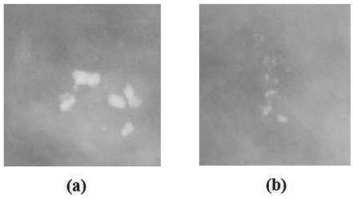

Fig. 1. Typical MC clusters: (a) benign, (b) malignant

[9], and fuzzy sets [10]. Most recent researches have been based on deep learning [11,12] and active contours [2]. In our proposed methods, a series a morphological operations were applied to segment MC clusters. Two different segmentation methods were proposed for MC cluster segmentation - where the second approach was built on the results of the first technique. The segmentation results have been compared with the MC cluster annotation delinated by an expert radiologist. Dice similarity metric [17,18] was calculated to obtain the similarity score of our proposed segmentation approaches with the reference mask. Beside this, the segmented images were used to extract features for generating a feature space which were used with an ensemble classifier to investigate the effectiveness of the extracted features for classification purposes.

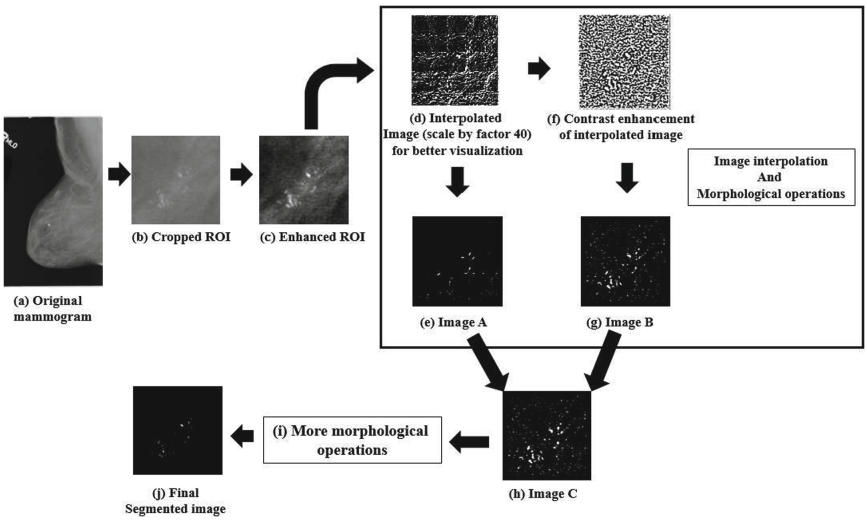

Fig. 2. Overview of the proposed approach.

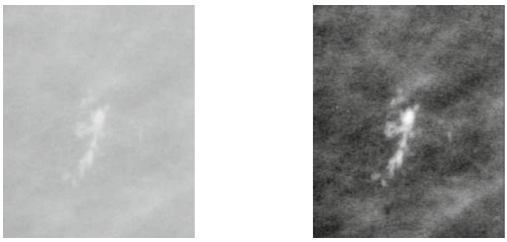

(a) (b)

Fig. 3. Enhancement of ROI: (a) original image, (b) enhanced MC cluster.

2 Materials and Methods

The overview of the proposed method is shown in Fig. 2, and described in details in the following sections. The developed techniques were applied, implemented, and tested on regions of interest (ROI), containing MC clusters which were selected by an expert radiologist. The proposed segmentation techniques were tested on the digitized mammograms from two different publicly available benchmark datasets: The Mammography Image Analysis Society (MIAS) [21]; and The Digital Database for Screening Mammography (DDSM) [22]. A total number of 248 digitized mammograms which contain MC clusters (131 benign and 117 malignant-biopsy proven), were extracted from DDSM, and 24 images (12 benign and 12 malignant) were extracted from MIAS, where the ground truth of the locations of the abnormalities were delineated by expert radiologists.

2.1 Enhancement of ROI

A wavelet-based algorithm [13] was used to enhance the ROIs. The number of sub-bands for image decomposition was chosen as 3 and the decomposition level was also set to 3, as we aimed to obtain the horizontal, vertical and diagonal details of the MC clusters. Moreover, each sub-band was assigned a predefined weight equal to 0.8 to enhance diagonal higher spatial frequency. An example enhanced MC cluster is shown in Fig. 3.

2.2 Image Segmentation

The MC patches were segmented using two different segmentation approaches. The results generated from these two distinct segmentation methods were later used for MC classification to evaluate which segmentation strategy obtained higher accuracy.

2.2.1 MC Clusters Segmentation Using Morphological Analysis

A combination of an interpolation method [14] and a sequence of morphological operations was used to segment the MC clusters. The entire image was initially

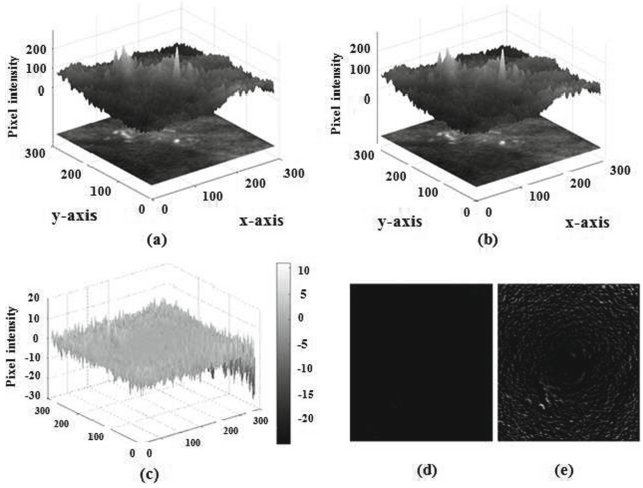

Fig. 4. (a) Three-dimensional intensity representation of a 300 × 300 pixel area, (b) calculated background intensity of the same area, (c) intensity difference between original and background pixel intensity values, (d) intensity difference image, (e) intensity difference image multiplied by a factor 25 for better visualization.

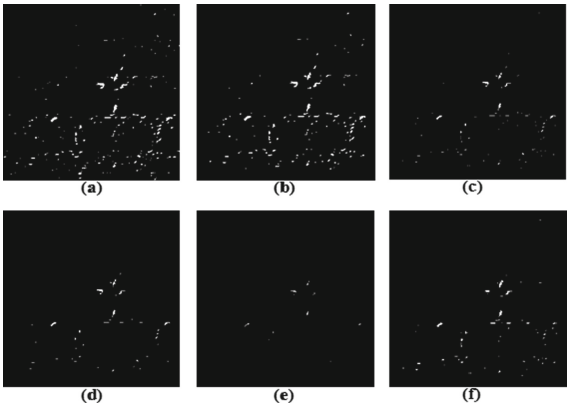

Fig. 5. (a) Binary image containing the highest positive 5% intensity values of the difference image, (b) after removing single pixels from (a), (c) after performing erosion, (d) eliminating single pixels from the eroded image, (e) result after eroding the single pixel removed image, (f) Image A: pixels that have higher values than the threshold are added to the eroded image.

split into sub-regions, and bi-cubic interpolation [14] was applied to each sub-region to obtain the intensity level of the local background. The interpolated image was subtracted from the original image to produce a difference image, see Fig. 4 for an image based explanation.

All pixels having positive value were identified from the difference image and the highest 5% intensity values were selected to produce a binary image, see Fig. 5(a). This provided a trade-off between under segmentation and over segmentation. A series of morphological operations were also used to reduce over segmentation. The resulted images of the morphological operations are shown in Fig. 5.

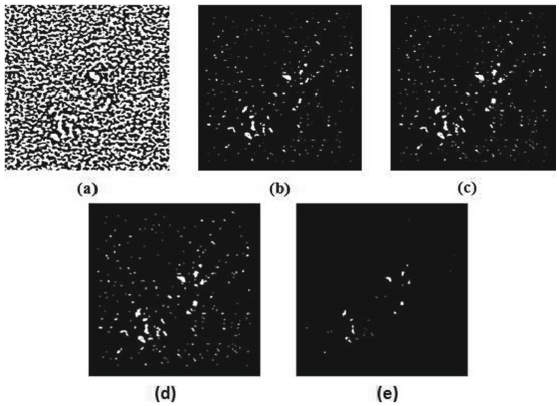

Fig. 6. (a) The result of applying contrast enhancement filter, (b) Image B: the highest 5% intensity pixels selected from the enhanced image, (c) Image C: logical summation of two binary images A and B, (d) 8-connected components kept from Image C, (e) the effects of erosion on 8-connected components.

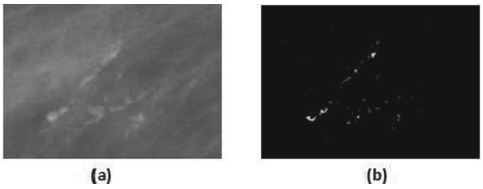

Fig. 7. Morphological approach based MC cluster segmentation: (a) Original image, (b) segmented MC cluster.

In parallel, a contrast enhancement filter was applied to the bi-cubic interpolated image, with a 9×9 kernel having its center pixel weight as 80 and all other elements as -1 [14], see Fig. 6(a). Afterwards, 5% highest intensity pixels were selected from the filtered image and were used to generate another binary image (labeled B in Fig. 6(b)). The logical AND operation of the two binary images-image A (Fig. 5(f)) and image B (Fig. 6(b)), was carried out to generate another binary image, (labeled C in Fig. 6(c)). A series of morphological operations were performed on Image C, to remove single pixel blobs - which are considered as

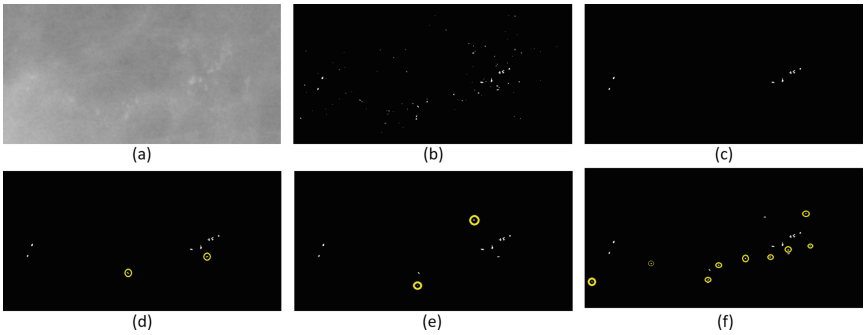

Fig. 8. (a) Original ROI (Benign: $B\_3030\_1.RIGHT\_MLO$), (b) segmented image generated using approach 1 (Having more then 20 blobs), (c) Image Y: keeping blobs that have area covered within the range of 50% of highest blob areas (the image has less then 20 blobs: blob count = 7, (d) MC cluster blob count: 9 (iteration: 1), (e) MC cluster blob count: 11 (iteration: 2), (f) MC cluster blob count: 20 (iteration: 4) which equals the final MC cluster segmentation using area ranking technique.

artifacts [15]. The neighboring pixels with 8-connectivity were grouped together to create candidate MC clusters, see Fig. 6(d) and an erosion operation was carried out with a 3×3 kernel of unit value, which removed small objects (see Fig. 6(e)). Subsequently, the total number of objects inside the image was calculated. If this number is less than the 5% of the total number of 8-connected component in, Fig. 6(d), then the area of all connected components in Fig. 6(d), were calculated and a binary image was generated that contained only the blobs that reside inside the range of 30% highest area values. The total number of blobs were kept above the 5% of the total number of 8-connected component, and the 30% highest area values were taken into account to obtain accurate segmented MC cluster.

Afterwards, the image- Fig. 6(d), was divided into 100×100 blocks to carry out a block processing operation. All the elements inside each 100×100 block were eliminated if the minimum number of objects inside the block is less than 3. The reason for considering the block size as 100×100 and selecting the minimum number of object inside each block as 3 was to follow the medical definition of the existence of clustered MC [16]. The rule has been used for the reduction of false positive detected ROIs and all the regions that include less than three objects were eliminated to generate the final segmented result, see Fig. 7.

2.2.2 MC Clusters Segmentation Using Area Ranking Technique

The second approach for MC cluster segmentation was based on the approach described in Sect. 2.2.1. The total number of individual MC was calculated from the segmented image. If the total number of individual MC is greater than 20, as shown in Fig. 8(b), then the area of all MC was calculated and ranked from highest to lowest order. Only the blobs of individual MC was taken into an account that had an area lies within the range of the 50% of highest MC area

of image Y (Fig. 8(c)). If image Y, contained less than 20 MC blobs, then the process of adding blobs to image Y was started and continued until a minimum of 20 blobs were included to generate the final MC cluster segmented Fig. 8(d–e). A minimum of 20 blobs was considered to avoid under segmentation.

3 Results and Discussion

The evaluation was carried out using the Dice similarity metric [17–19]. The reference masks, see Fig. 9(b), were generated from the radiologist's annotation outline, see Fig. 9(a). Afterwords, the blobs of MC clusters that reside inside the radiologist's annotation were considered to generate convex hull. This convex hull, see Fig. 9(f), and the reference mask, see Fig. 9(b), were used to calculate the Dice similarity score. See Fig. 9. The Dice similarity metric for DDSM and MIAS is presented Fig. 10.

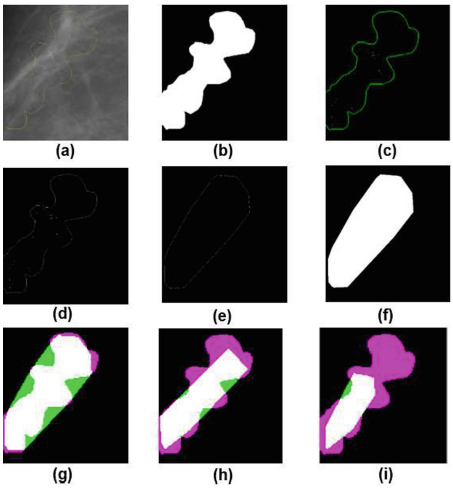

Fig. 9. (a) Annotation by radiologist ($B\_3121\_1.RIGHT\_MLO$), (b) reference MC cluster mask generated from (a), (c) border extraction from reference MC mask and overlaid on segmented image generated using morphological segmentation approach, (d) MC resides inside the border annotated by expert radiologist, (e) convex hull outline using the border points of segmented blobs residing inside annotation outline, (f) mask generation from convex hull border of segmented image, (g) Dice similarity score (based on morphological segmentation approach) = 0.85599; White region = True positive, Green region = False positive, Magenta region = False negative, (h) Dice similarity score (based on Oliver's [7] segmentation approach) = 0.76514, (i) Dice similarity score (based on area ranking segmentation approach) = 0.5494.

From Fig. 10, it is clear that the segmentation technique based on morphological approach works better than the area rank based segmentation method.

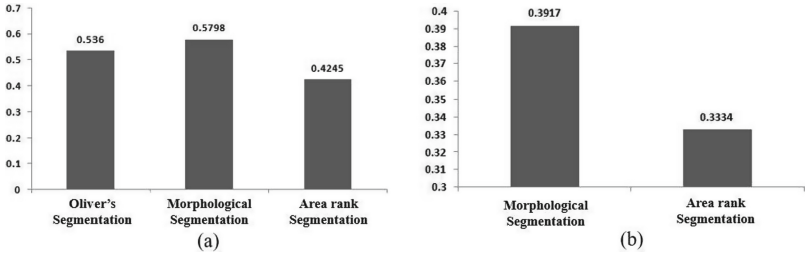

Fig. 10. (a) Dice similarity score to compare segmentation results of Oliver's segmentation method, and our proposed two segmentation methods using DDSM database (b) Dice similarity score to compare segmentation results of our proposed two segmentation methods using MIAS database

Table 1. Classification of segmented image using a 10-fold cross-validation approach.

Method	Database	Result
Oliver et al. [7]	DDSM	AC = 94.11 ± 0.48%,
		Az = 0.94 ± 0.01
Morphological approach based segmentation	DDSM	AC = 94.48 ± 1.11%,
		Az = 0.94 ± 0.01
Area rank based segmentation	DDSM	AC = 75.36 ± 1.61%,
		Az = 0.74 ± 0.02
Morphological approach based segmentation	MIAS	AC = 100.00 ± 0.00%,
		Az = 1.00 ± 0.00
Area rank based segmentation	MIAS	AC = 74.58 ± 4.35%,
		Az = 0.75 ± 0.04

Also, it is to be noted that, the segmentation results generated by applying the method of Oliver et al. [7] gives almost the same similarity score as gained by our proposed morphological opeation based segmentation method - though the similarity score for our proposed approach is slightly higher than Oliver's method [7]. The reason for getting almost the same similarity score for our approach and Oliver's method [7] was because the similar number of blobs sequenced.

To investigate further the accuracy of the developed segmentation approaches, an ensemble classifier was used to observe how accurate MC clusters could be classified while using the segmented images. A set of 51 features was extracted, and a union of the 15 most important features from both segmentation approaches and Oliver's method [7] were considered to create the feature space used by the ensemble classifier using 10-fold cross-validation [20]. The classification result using the segmented MC clusters are shown in Table 1. From Table 1, it is to be noted that the classification accuracy for segmentation based on morphological operaration technique and Oliver's method [7] have

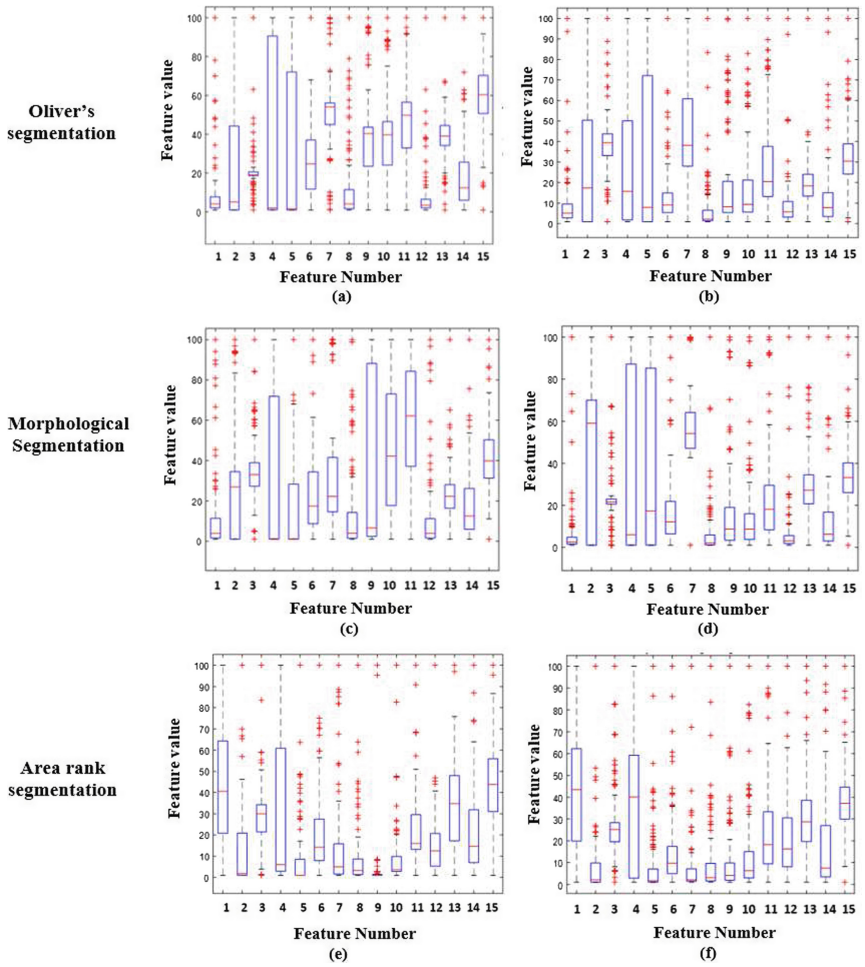

Fig. 11. Box plot showing the whiskers of 15 significant features extracted from three different segmentation approach on DDSM database.

almost similar results whereas the classification accuracy for area rank based segmentation approach has drastically decreased.

Figure 11 shows the distribution of feature values for benign and malignant MC clusters to inspect the reason of getting higher accuracy for our proposed segmentation approach (based on morphological analysis) and Oliver's method [7]; and getting a sharp fall in the accuracy whilst using the segmented image generated by area rank based segmentation approach. The first, second, and third rows represent the segmentation methods which were used to generate the images from where the features were extracted. Moreover, the first and second columns represent the malignant and benign features, respectively. From Fig. 11, while comparing the interquartile range (IQR) of the feature values that where

extracted from Oliver's segmentation method [7] with our proposed morphological analysis based segmentation method, it was found that there are significant fluctuations in the IQR of feature no: 3, 6, 7, 9, 10, 15 for malignant and benign features. Furthermore, a notable disparity in whisker spans were also observed for the said features. Feature no: 3, 6, 7, 9, 10, and 15 represent elongation, entropy, individual MCs distance from MC cluster centroid, MC cluster area, MC cluster perimeter, sobel gradient direction, respectively. Such difference in whisker and IQR of features eventually influence the classification scenario and results in the highest accuracy when using the segmented image obtained by applying our proposed morphological segmentation based method. Furthermore, when considering the scenario for the segmented images generated from area rank based approach, it is found that there were less variation in the range of whisker and IQR for benign and malignant case that eventually resulted the lowest classification accuracy.

4 Conclusions

The paper has presented a new technique for MC cluster segmentation using a series of morphological operations. The proposed approach was focused on the improvement of the accuracy of MC cluster segmentation to facilitate the final output of a CADx pipeline, by selecting the most salient features from the segmented image. The proposed method was evaluated using MIAS and DDSM. Two different approaches are proposed to segment the MC clusters. The morphological operation based segmentation approach showed the highest Dice metric similarity score (0.6192). The segmented image generated using the same proposed approach also showed the highest classification accuracy ($94.48 \pm 1.11\%$).

References

1. Breast Cancer Statistics. https://breast-cancer.canceraustralia.gov.au/statistics. Accessed 14 Feb 2018
2. Duarte, M.A., Alvarenga, A.V., Azevedo, C.M., Calas, M.J.G., Infantosi, A.F., Pereira, W.C.: Evaluating geodesic active contours in microcalcifications segmentation on mammograms. Comput. Methods Programs Biomed. **122**(3), 304–315 (2015)
3. Sridhar, B., Reddy, K.V.V.S., Prasad, A.M.: Detection of lesions in medical image using an artificial neural networks and morphological filters. Comput. Sci. Telecommun. **43**(3), 12–19 (2014)
4. Arodz, T., Kurdziel, M., Popiela, T.J., Sevre, E.O., Yuen, D.A.: Detection of clustered microcalcifications in small field digital mammography. Comput. Methods Programs Biomed. **81**(1), 56–65 (2006)
5. Betal, D., Roberts, N., Whitehouse, G.H.: Segmentation and numerical analysis of microcalcifications on mammograms using mathematical morphology. Br. J. Radiol. **70**(837), 903–917 (2000)
6. Halkiotis, S., Botsis, T., Rangoussi, M.: Automatic detection of clustered microcalcifications in digital mammograms using mathematical morphology and neural networks. Sig. Process. **87**(7), 1559–1568 (2007)

7. Oliver, A., Torrent, A., Lladó, X., Tortajada, M., Tortajada, L., Sentís, M., Freixenet, J., Zwiggelaar, R.: Automatic microcalcification and cluster detection for digital and digitised mammograms. Knowl.-Based Syst. **28**, 68–75 (2012)
8. Chen, Z., Strange, H., Oliver, A., Denton, E.R., Boggis, C., Zwiggelaar, R.: Topological modeling and classification of mammographic microcalcification clusters. IEEE Trans. Biomed. Eng. **62**(4), 1203–1214 (2015)
9. Batchelder, K.A., Tanenbaum, A.B., Albert, S., Guimond, L., Kestener, P., Arneodo, A., Khalil, A.: Wavelet-based 3D reconstruction of microcalcification clusters from two mammographic views: new evidence that fractal tumors are malignant and Euclidean tumors are benign. PloS One **9**(9), e107580 (2014)
10. Mohanalin, J., Kalra, P.K., Kumar, N.: Microcalcification segmentation using normalized Tsallis entropy: an automatic "q" calculation by exploiting type II fuzzy sets. IETE J. Res. **55**(2), 90–96 (2009)
11. Samala, R.K., Chan, H.P., Hadjiiski, L.M., Cha, K., Helvie, M.A.: Deep-learning convolution neural network for computer-aided detection of microcalcifications in digital breast tomosynthesis. In: Medical Imaging 2016: Computer-Aided Diagnosis, vol. 9785, p. 97850Y (2016)
12. Wang, J., Yang, X., Cai, H., Tan, W., Jin, C., Li, L.: Discrimination of breast cancer with microcalcifications on mammography by deep learning. Sci. Rep. Ann. Stat. **6**, 27327 (2016)
13. Mishra, S., Patra, R., Pattanayak, A., Pradhan, S.: Block based enhancement of satellite images using sharpness indexed filtering. IOSR J. Electron. Commun. Eng. **8**, 20–24 (2013)
14. Papadopoulos, A., Fotiadis, D.I., Likas, A.: Characterization of clustered microcalcifications in digitized mammograms using neural networks and support vector machines. Artif. Intell. Med. **34**(2), 141–150 (2005)
15. Chan, H.P., Lo, S.C.B., Sahiner, B., Lam, K.L., Helvie, M.A.: Computer aided detection of mammographic microcalcifications: pattern recognition with an artificial neural network. Med. Phys. **22**(10), 1555–1567 (1995)
16. Kopans, D.B.: Breast Imaging. Lippincott Williams and Wilkins, Philadelphia (1989)
17. Srensen, T.: A method of establishing groups of equal amplitude in plant sociology based on similarity of species and its application to analyses of the vegetation on Danish commons. Biol. Skr. **5**, 1–34 (1948)
18. Dice, L.R.: Measures of the amount of ecologic association between species. Ecology **26**(3), 297–302 (1945)
19. The SrensenDice index. https://en.wikipedia.org/wiki/S%C3%B8rensen%E2%80%93Dice_coefficient#cite_note-zijdenbos-6. Accessed 2 Feb 2018
20. Alam, N., Zwiggelaar, R.: Automatic classification of clustered microcalcifications in digitized mammogram using ensemble learning. In: 14th International Workshop on Breast Imaging (IWBI 2018), vol. 10718, p. 1071816. International Society for Optics and Photonics (2018)
21. Suckling, J., Parker, J., Dance, D., Astley, S., Hutt, I., Boggis, C., Ricketts, I., Stamatakis, E., Cerneaz, N., Kok, S., Taylor, P.: Mammographic Image Analysis Society (MIAS) database v1. 21 (2015)
22. Heath, M., Bowyer, K., Kopans, D., Kegelmeyer, P., Moore, R., Chang, K., Munishkumaran, S.: Current status of the digital database for screening mammography. In: Karssemeijer, N., Thijssen, M., Hendriks, J., van Erning, L. (eds.) Digital Mammography. CIVI, vol. 13, pp. 457–460. Springer, Dordrecht (1998). https://doi.org/10.1007/978-94-011-5318-8_75